9. Monitoring dispersion and re-agglomeration phenomena during the manufacture of polymer nanocomposites

José A. Covas and Maria C. Paiva

9.1 Introduction

Polymer nanocomposites consist of a polymer matrix and reinforcing particles that have at least one dimension under 100 nm [1]. It has been extensively reported that the incorporation of a small amount of a nanofiller (typically 3–5 wt%) may attain the same reinforcement level as 20–30 wt% of the same micro-sized filler [2]. Not surprisingly, the development of nanocomposites has been a dynamic area of research for more than three decades. Layered clays (in particular, montmorillonite), carbon nanotubes and graphene derivatives have been the most studied fillers given their inherent outstanding properties. The interest in this area of research started with polymer-clay nanocomposites in the late 80s, followed by polymer-carbon nanotube composites in the late 90s and with graphene based composites since around 2006 [2].

The performance of these nanocomposites depends on the properties of their constituents, on their composition and on various characteristics of the nanoparticles such as size, aspect ratio, specific surface area, and physical/chemical compatibility with the matrix. The degree of dispersion of the nanoparticles within the polymer is particularly influent upon the composite properties. All nanoparticles, having a large surface-to-volume ratio, tend to agglomerate and form macroscopic clusters that are detrimental to the composite properties. Nanoparticle surface modification to enhance the compatibility of the matrix and fillers is often used as a means to aid their dispersion in the polymer. Despite the intensive research, achieving the adequate level and uniformity of nanoparticle dispersion remains a practical challenge. However, in order to explore the full potential of properties enhancement provided by the various types of particles (e.g., flame retardancy, mechanical, barrier, electrical, thermal properties), dispersion of the nanoparticles in the matrix is necessary. This has hindered the wider application of carbon nanotubes and graphene, which are costlier than clays.

Various routes have been developed to manufacture polymer nanocomposites. In-situ polymerization of the monomer in the presence of an initiator and the filler allows the production of composites with high filler loadings and good filler dispersion. In solution processing filler, surfactant and polymer are mixed in a suitable solvent, followed by evaporation of the latter. Melt mixing consists in the physical/mechanical mixing of the filler with the polymer in the melt state. This method is the most suitable for industrial production as it uses commercial processing equipment, often twin screw extruders that are capable of high outputs and automated production, and avoids the use of solvents. It has been demonstrated that polymer nanocomposites prepared by this technique normally contain nanoparticle agglomerates (typically smaller than the nanoparticle agglomerates in the

powder form) together with individually dispersed particles, and that the final degree of dispersion depends on the mixing method and operating conditions.

Many studies have focused on establishing correlations between melt mixing conditions, the resulting dispersion and associated performance of the composite materials. Studies aiming at unveiling the dispersion mechanisms of the various types of fillers are less abundant. Monitoring the actual progress of dispersion along the length of mixers in order to ascertain the role of thermal and rheological effects is even less common. This chapter analyses the dispersion of layered silicates, carbon nanotubes and graphene derivatives by melt mixing. Both the general mechanisms and the progress of dispersion along the axis of the mixer will be discussed. The possibility of partial reversion of dispersion due to thermal effects and/or stress relaxation effects will be demonstrated.

9.2 ORGANOCLAYS

Nanoclays are nanoparticles of layered mineral silicates, normally organized into classes such as montmorillonite, bentonite, kaolinite, hectorite, and halloysite, according to their chemical composition and nanoparticle morphology. Montmorillonite (MMT), a smectite type of clay, is probably the most widely used layered silicate for the manufacture of nanocomposites because it is abundant and thus inexpensive. Layered silicates are usually available as stacks of tactoids and have hydrophilic character. The lateral dimension of each individual clay platelet may be as large as 10 µm (depending on clay type), while the thickness is approximately 1 nm, corresponding to a surface area reaching 750–800 m²/g. The modulus of each MMT platelet is approximately 178-220 GPa [3].

Polymer-clay nanocomposites are expected to present high mechanical performance, thermal stability, barrier characteristics and fire retardation properties (compared to the polymer matrix alone) at clay loadings typically below 5 wt.%. To attain those properties, dispersion of the tactoids in a polymer melt should ideally achieve total delamination (usually known as exfoliation) of the individual platelets. In practice, this is hindered by:

- the Van der Waals interactions between individual platelets, leading to strong interaction;
- the incompatibility with non-polar hydrophobic polymers; in their pristine state, layered silicates are miscible only with hydrophilic polymers, such as poly(ethylene oxide) (PEO) [4] or poly(vinyl alcohol) (PVA) [5]; to make silicate particles miscible with most polymer matrices, their hydrophilic surface must be converted into an organophilic one, which will facilitate the diffusion of the polymer chains within the clay interlayer spacing (a process known as intercalation). This is often achieved by ion-exchange reactions with cationic surfactants (including primary, secondary, tertiary, and quaternary alkyl ammonium or alkylphosphonium cations) that yield an organophilic clay where alkyl-ammonium or phosphonium cations are intercalated within the layers, resulting in a larger intergallery spacing [3];
- the often limited thermal stability of clay surfactants; although the selection of the surfactant architecture is usually made by taking into account the nature of the polymer matrix, if the compounding/processing temperature is too high decomposition occurs; this will affect the interfacial interaction between filler and matrix and, consequently, the dispersion characteristics, as will be discussed below in greater detail.

9.2.1 Dispersion of layered clays

The extent of clay dispersion will vary depending on the interaction between polymer and clay surface, as well as on the thermomechanical stresses applied during melt mixing. The process initiates with the diffusion of the polymer chains within the clay interlayer spacing (intercalation stage), followed by the delamination of the individual platelets (exfoliation stage) and their diffusion into the melt [6, 7]. Figure 9.1 represents schematically the different polymer-clay morphologies that may result from melt mixing. Microcomposites are obtained when the polymer is unable to diffuse into the interlayer spacing (also denoted as clay galleries), i.e., the clay remains in its agglomerate state, creating a micro-dispersed phase. The corresponding properties are comparable to those of conventional microcomposites. An intercalated nanocomposite exhibits a multilayer morphology due to the diffusion of the polymer chains into the interlayers, whose spacing is approximately 2 – 4 nm [6,8,9]. An exfoliated morphology consists of individual clay platelets suspended in a polymer melt (the distance between them exceeding 8 – 10 nm [6,8-10]). In the latter case the polymer–clay interphase area is maximized, and so is the performance of the material. In principle, exfoliation could be attained through the sliding of adjacent platelets followed by diffusion of the polymer chains into the clay galleries and/or by peeling of the platelets, starting from the edges. In practice, polymer–clay nanocomposites produced by melt mixing – the method generally adopted at the production scale - present a mixed morphology, containing intercalated clay tactoids and exfoliated platelets.

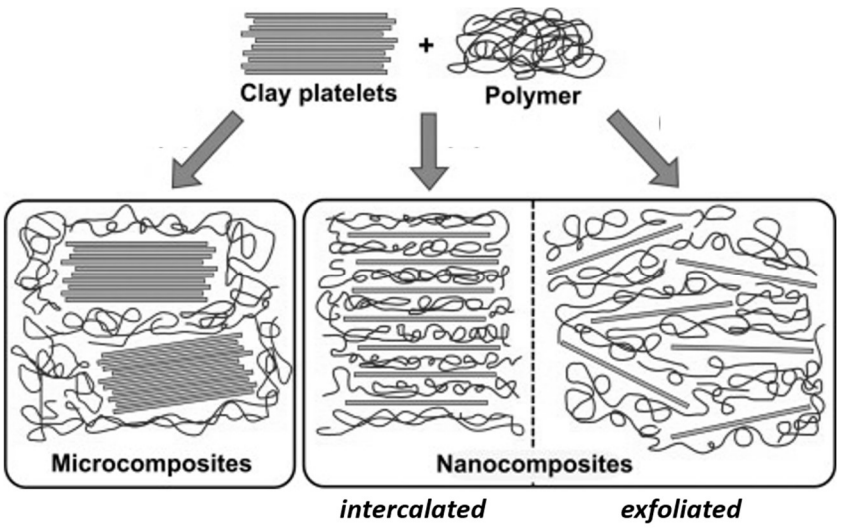

Figure 9.1 Schematic representation of the polymer-clay morphologies that can result from the dispersion by melt mixing of layered organoclays in polymer matrices.

As for other polymer nanocomposites, assessing the degree of clay dispersion in a polymer matrix is not straightforward. In practice, it is usually accomplished using one or more of the following techniques: i) direct observation of the morphology by transmission electron microscopy - this technique analyzes minute areas, becoming time consuming and almost impossible to obtain statistically relevant data; ii) X-ray diffraction - a convenient technique with the limitation that the maximum detectable interlayer spacing is 8 nm; iii) Fourier-transform infrared spectroscopy (FT-IR), which can detect peak shifts in the Si-O region; and iv) rheological response of the composite in oscillatory rheometry under small amplitude oscillatory shear (SAOS). These techniques probe different effects, and some relevant aspects related to their application are given below (9.2.2).

Bousmina [7] showed that the diffusion of polymer chains inside the clay galleries is improved under mild shearing conditions (polymer with medium to low viscosity) applied during sufficient time, whereas extensive exfoliation requires a high level of shearing/deformation. When proper chemical affinity exists between polymer and clay, exfoliation can develop even at low shear rates. When using twin-screw compounding for the manufacture of polymer-clay nanocomposites, it is usually reported that high screw speeds promote dispersion due to the higher hydrodynamic stresses induced by the greater shear rates [6, 11-17], however contrasting results have also been reported [18,20]. Low feed rates may improve exfoliation due to the consequent increase of residence time [6,12,13,17]. High processing temperatures are often considered as detrimental for dispersion not only because they induce lower viscosities, but can also cause degradation of the clay surfactant (and, eventually, of the polymer matrix), which decreases the compatibility with the polymer matrix [6,11,20]. Vergnes et al. [12,13] observed that extrusion conditions (feed rate, screw speed and set temperature) have limited effect on intercalation, but high screw speeds and low feed rates induce higher final exfoliation levels. The current general view is that a balance between hydrodynamic stresses and residence time for polymer melt diffusion inside the layer spacing is required to achieve proper dispersion [6,7,11-13,15,21].

9.2.2 Monitoring the development of dispersion

Since clay dispersion is a gradual process, the analysis of its evolution along the axis of the extruder is essential to understand the underlying mechanisms involved. This type of information is also useful for practical process set-up and optimization. However, the literature on the topic is scarce. Lertwimolnun and Vergnes [13] characterized post-mortem samples of a PP/clay system removed from various locations along the extruder screw. They found that dispersion reached relatively high levels immediately after polymer melting, then it could progress, remain constant or regress downstream, depending on operating conditions and/or screw design. Regression of dispersion was ascribed to matrix degradation. The characterization of post-mortem samples has been often adopted to study the evolution of physico-chemical phenomena along the extruder. The technique requires interrupting the extrusion process, is time consuming, and could lead to misleading conclusions. In fact, during the extraction of the screws (which takes several minutes) the material remains subjected to no-flow conditions at high temperature, which favour relaxation phenomena – with consequent changes in morphology - and/or further conversion of chemical reactions. In order to circumvent these limitations, Machado et al [22] modified the barrel of a co-rotating twin screw extruder to include collection points along the screw length. During normal operation it became possible: i) to collect quickly (and immediately freeze for subsequent characterization) material samples from selected locations along the barrel and ii) to perform in-process measurements (on-line NIR, on-line oscillatory and capillary rheometry) that could be correlated to the local extent of dispersion. Using this equipment coupled to on-line oscillatory rheometry and in-line NIR, the evolution of dispersion during the preparation of a PP/ PP-g-MA/organoclay system by twin screw compounding was studied using three different screw configurations [23]. The prototype on-line oscillatory rheometer [24] operated in small amplitude oscillatory shear (SAOS) and measured the storage and loss moduli (G', G") and the melt yield stress (σ_0). An increase of the elastic modulus at low frequencies is generally attributed to a fine nanoclay dispersion, whereas an increase of the yield stress or of the power law index was correlated with exfoliation [12,15,20,24-26]. The in-line Near-Infrared (NIR) spectroscopy set-up used a reflectance probe [27]. Through adequate chemometrics, the absorbance spectra acquired was related to dispersion intensity by a 7-parameter regression model, which combines four rheological properties (G', G", σ_0 and the power law index), two Fourier transform-Infrared spectroscopy (FT-IR) parameters (wavenumber shifts for the peaks at 1050 cm^{-1} and 1080 cm^{-1}, usually associated to intercalation and exfoliation, respectively [28-30]) and a thermomechanical index related to the mechanical energy input to the system (specific mechanical energy, SME) [27].

Regardless of the screw profile, the two techniques (SAOS and NIR) indicated a significant progress in dispersion of the PP/ PP-g-MA/organoclay system upon melting of the polymer immediately upstream of the first mixing zone, due to intense shear and complex velocity profiles along several screw turns. Further downstream, dispersion was found to level off and/or decrease, even if the final dispersion levels were significant (See Fig 9.2a). Scanning Transmission Electron Microscopy (STEM) studies and X-ray diffraction (XRD) patterns of nanocomposite samples confirmed these observations. As the material progresses downstream, the cumulative residence time increases while the hydrodynamic stresses are lower than those developing upon melting, given the higher local temperatures. Therefore, degradation of the matrix or of the clay surfactant could play a role in the progress of dispersion. The former would entail a decrease of the viscosity, which could enable the diffusion of the melt out of the clay interlaying spaces, and the eventual collapse of the platelet network. In turn, the lower distance between individual platelets could also prompt some re-agglomeration. Surfactant degradation would decrease the interlaying spaces and the interaction with the matrix, thus causing similar effects.

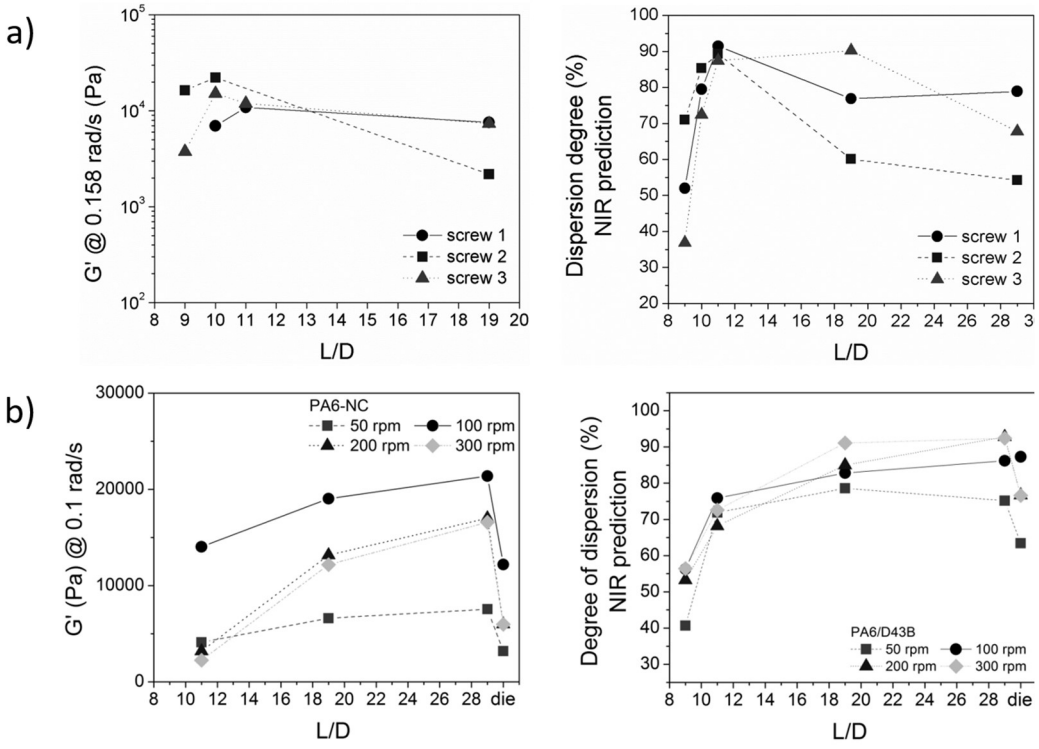

Figure 9.2 Evolution of dispersion along the axis of a twin screw extruder, as measured by SAOS (G') and NIR: a) PP/ PP-g-MA/organoclay (adapted from [23]); b) PA6/organoclay (adapted from [32]).

Thermogravimetry (TGA) and Time of Flight-Secondary Ion Mass Spectrometry (TOF-SIMS) of the matrix, organoclay and nanocomposites demonstrated that degradation of the clay surfactant took place even at low processing temperatures, triggering the subsequent degradation of the polymer matrix [23]. For example, isothermal TGA tests revealed that while at 150 ºC the organoclay suffered a minor weight loss lower than 0.05%, at 180 ºC and 200 ºC the weight loss increased to 1.8 wt% and 3.5 wt% respectively, due to the decomposition of the alkylammonium modifier. In parallel, the TOF-SIMS spectrum of the

nanocomposite suggested degradation of the matrix by chain scission. Nassar et al. [31] and Shah and Paul [20] postulated that the α-olefins formed by degradation of the alkyl tails of the surfactant readily react with oxygen to form peroxides, which will eventually trigger chain scission. The authors observed that viscous dissipation could generate matrix degradation. Consequently, both thermal degradation of the clay surfactant and of the polymer matrix may contribute to the observed reversion of dispersion along the extruder.

Therefore, a proper combination of hydrodynamic stresses and residence time will quickly create high levels of dispersion, originating intercalation and exfoliation. However, as explained above, degradation of the clay surfactant may lead to re-stacking of the intercalated clay layers, while matrix degradation leads to viscosity decrease, which will reduce the stress level. Thus, for the purpose of organoclay dispersion in twin screw extruders, there is little advantage in using long L/D screws ratios, or fit screws with highly restrictive mixing zones downstream.

The above conclusions were attained using a non-polar polymer, polypropylene, with little compatibility with this type of fillers. Accordingly, it is interesting to examine whether the use of a polar polymer such as polyamide 6 will generate similar effects [32]. As before, substantial dispersion levels were reached in the first mixing zone of the screw, concurrently with melting of the polymer. In the second part of the extruder, dispersion either continued or remained constant up to the screw tips, i.e., no reversion was detected. However, a pronounced decline of the degree of dispersion at the die exit was observed for all processing conditions tested. This was attributed to the significant viscous dissipation occurring along the die, causing degradation of the clay surfactant and chain scission of the polyamide 6 matrix, as demonstrated by NIR, rheology and X-ray diffraction (see Fig. 9.2b). Degradation reduces polymer-clay affinity which, together with the lower melt viscosity due to higher temperature, enables diffusion of the polymer chains out of the clay galleries, causing the partial collapse of the intercalated structure.

In summary, the conventional mechanism of layered clays dispersion in polymers proposing the formation of microcomposites, intercalated and/or exfoliated nanocomposites, illustrated in Fig. 9.1, can be further completed to account for reverse dispersion phenomena. As schematized in Figure 9.3, clay nanocomposites produced by melt mixing techniques combine intercalated an exfoliated structures. Complete intercalation may be difficult to achieve as the tactoids may collapse, at least partially, due to continuing shear and surfactant degradation. The process complexity interferes with the dispersion kinetics explaining, at least partially, why conflicting correlations between dispersion and processing conditions have been widely reported for extrusion processing. Monitoring the evolution of dispersion along the extruder axis was fundamental to assess the role of the surfactant/polymer degradation on the dispersion of nanoclays in polymers.

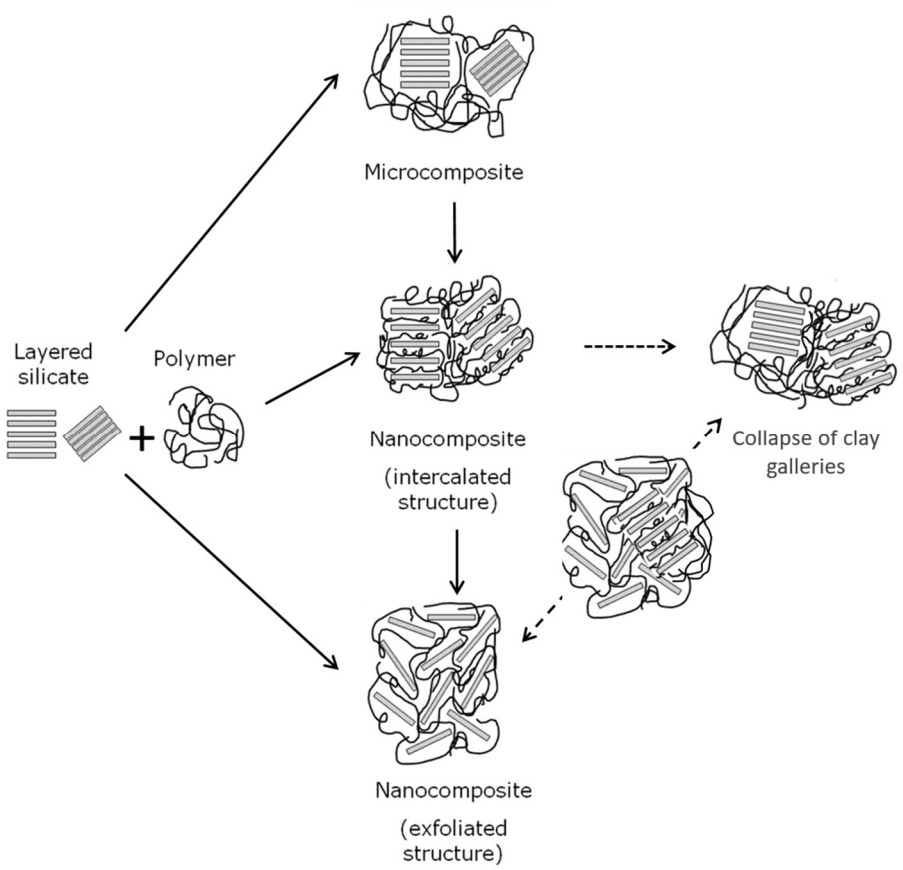

Figure 9.3 Dispersion mechanism of layered organoclays into polymer matrices taking into account the possible collapse of the clay galleries due to the thermal degradation of the clay surfactant and polymer.

9.3 Carbon Nanotubes

Carbon nanotubes (CNT) are formed by a hexagonal lattice of sp2 hybridized carbon atoms wrapped into a cylindrical shape. CNT can be formed as single-walled (SWCNT) or multi-walled (MWCNT), the former consisting of an individual graphene layer rolled-up into a cylindrical shell with a diameter of 1–2 nm, whereas the latter contains several cylindrical shells coaxially arranged and stacked, separated by a distance of 0.34 nm. CNT have outstanding mechanical and thermal properties, with typical values for Young's modulus of 1 TPa, tensile strength > 50 GPa, thermal conductivity > 3000 W m^{-1} K^{-1} and electrical conductivity in the range 10^{6}–10^{7} S m^{-1}. This set of excellent properties makes them attractive for applications in conductive polymer composites and adhesives, energy storage, thermal conductors, structural composite materials, microelectronics, etc [33,34]. However, practice demonstrated that attaining full performance is not easy, not only because commercial CNT contain impurities (e.g., metal catalyst particles and amorphous carbon), lack dimensional uniformity, form stable agglomerates and are difficult to disperse in polymer matrices. This created a trough of disillusionment in the 2000's, questioning their commercial sustainability. In recent years, a better understanding of the chemical-physical characteristics and dispersion mechanisms, together with advances in manufacturing

technologies and in surface functionalization, promoted a new upsurge in the practical interest in CNT.

The dispersion of carbon nanoparticles in polymeric matrices is difficult because:

- In the pristine state, π-π stacking and van der Waals interactions between individual tubes may lead to significant attraction and formation of stable agglomerates;
- MWCNTs grow as highly entangled agglomerates of several microns or even millimeters;
- The surface chemical inertia of CNT due to the lack of chemical functionalities prevents the creation of strong interfaces with polymer molecules.

Interestingly, it is now generally accepted that perfectly dispersed CNT are required for maximum mechanical reinforcement, however the existence of a few agglomerates is not always detrimental and may be necessary to build-up an effective conductive network. Consequently, the survival of initial agglomerates or the development of secondary agglomerates during mixing with a polymer may be advantageous for electrical conductivity. Therefore, understanding the dispersion mechanisms of CNT is of major importance for the pratical production of nanocomposites with tailored CNT dispersion extent to achieve optimal performance.

Dispersion of CNT may be facilitated by surface modification of the particles and/or compatibilization with the polymer matrix (albeit this strategy may affect the transport properties). Chemical modification can be accomplished by non-covalent and covalent approaches [35,36]. Through electrostatic, van der Waals, or π-π stacking interactions, the former enables the attachment and stabilization of different functional groups at the surface of the CNT without disturbing its carbon structure and electronic network. However, this method is unsuitable for melting mixing - which is the focus of this chapter – as the functionalization compounds are usually unstable at the typical polymer processing temperatures. Covalent functionalization involves bonding chemical groups to the carbon atoms of the CNT surface, changing their hybridization state and decreasing their conjugation through the formation of covalent bonds. This method may induce surface damage and affect the electrical conductivity, however if the covalent functionalization approach is conveniently selected, the resulting functionalized CNT are appropriate for melt mixing.

9.3.1 Dispersion of Carbon Nanotubes

The dispersion of CNT in thermoplastic polymers during melt mixing has been the focus of numerous studies, using various types of mixing equipment and processing conditions. These studies converged to a number of general observations that enabled to build-up phenomenological dispersion models such as that illustrated in Figure 9.4. Dispersion of the CNT agglomerates requires their wetting and infiltration by the polymer melt, reducing the agglomerate cohesion strength. The ease of infiltration of the polymer melt depends mainly on the agglomerate density and size [37], on the polymer interfacial tension [38] and viscosity. Pötschke and co-workers [39-42] found a correlation between dispersibility of CNT and bulk density of the initial CNT agglomerates. Similarly, Salzano de Luna et al. [43] observed that CNT particles consisting of small and loosely packed clusters formed by interwoven bundles of combed yarns of nanotubes were easier to disperse then the reference denser commercial counterparts. Interfacial tension is not relevant when the hydrophobic CNTs are to be dispersed in polar polymers (e.g., polyamide, polycarbonate, polyimide). In the case of non-polar polymers (e.g., polyolefins), it is necessary to incorporate surface functionalities to the CNT as mentioned above.

If the magnitude of the hydrodynamic stresses (shear/extensional) is higher than the cohesive strength of the agglomerates, their size will reduce either by rupture and/or erosion. Rupture involves the successive break-up of the agglomerates into smaller ones and, ultimately, into the individual nanotubes. Erosion consists in the detachment of CNT, or small CNT agglomerates, from the surface of larger agglomerate clusters. While rupture is a fast process, erosion requires a long time to produce a comparable effect. Estimates of inter-tube binding forces suggest that high shear energy input is required to induce complete dispersion of the CNT, however at the cost of unwanted fiber breakage [44]. In practice, polymer/CNT nanocomposites prepared by melt mixing normally contain CNT agglomerates that are smaller than the initial agglomerates, together with individual nanotubes [45,47,48].

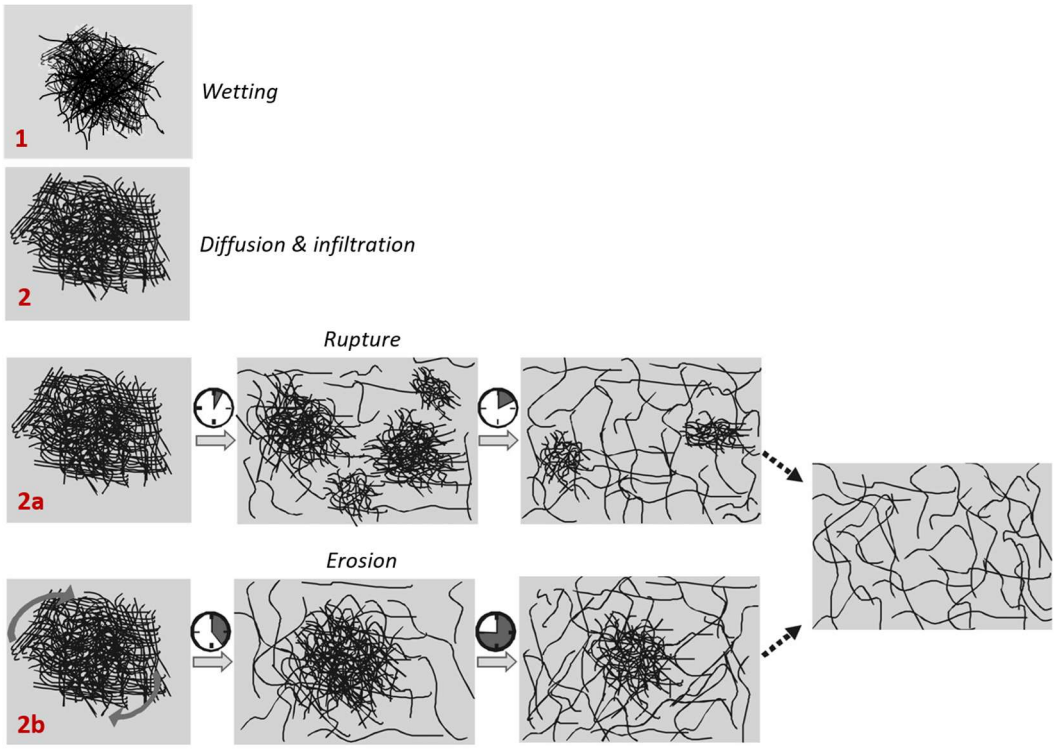

Figure 9.4 Dispersion mechanisms of CNT agglomerates in a polymer melt (adapted from [45,48]).

Scurati et al. [49] studied the behaviour of suspensions containing clusters of solid particles and defined a fragmentation number (Fa) that balances the hydrodynamic stresses (proportional to viscosity and shear rate) against the agglomerate cohesive strength. In the specific case of a polymer/silica particles system, it was experimentally observed that dispersion did not occur for $Fa < 2$, that the silica agglomerates eroded for $2 \leq Fa < 5$ and that rupture became the predominant mode of dispersion for $Fa \geq 5$. Even for sufficiently high Fa, there is a finite probability associated to the break-up process that is proportional to the residence time and the agglomerate surface area [50]. Although critical Fa have not yet been estimated for CNT, this concept appears adequate to describe their dispersion mechanism.

The influence of processing conditions on CNT agglomerate dispersion when using twin screw extruders for mixing has been extensively investigated [37,46,47,51-53]. It was observed that dispersion improves with increasing screw speed due to the associated higher stress levels generated. However, viscous dissipation may induce degradation which leads to deterioration of the composite performance. Increasing the throughput causes reduction of the residence time and an increase of the degree of screw fill, both hindering dispersion.

Barrel set temperatures determine the composite viscosity: in principle, lower melt viscosity facilitates infiltration into the CNT agglomerates, whereas higher viscosity should generate the higher hydrodynamic stresses required for rupture. Thus, the selection of processing parameters is paramount to optimize the dispersion of CNT agglomerates in the polymer melt.

9.3.2 Monitoring the development of dispersion

The CNT agglomerate dispersion mechanisms presented above were based on extensive analysis of experimental results, varying the process parameters and observing the resulting agglomerates morphology. As mentioned before for organoclays, monitoring the CNT agglomerates dispersion along the length of the mixer is expected to elucidate the dispersion mechanisms, and may provide information about the rate of dispersion, thus offering a more accurate description of the phenomena involved [37,53-55].

Figure 9.5a shows the evolution of the CNT agglomerates dispersion in polypropylene in terms of the average agglomerate size variation along the length of a prototype extensional mixer. The mixer consists of a vertical stack of circular channels with alternating small/large diameters, and thus the position along the mixer is labelled as the number of pairs of rings [54]. The assemblage sits at the bottom of a capillary rheometer, so that when the ram descends at a controlled speed forcing the composite melt through the mixer, a sequence of repetitive convergent/divergent flows is generated. It is well recognized that the normal stresses that are produced, superimposed on the shear stresses, are effective for dispersion [54-57]. Mixing was performed at the average shear rates (in the smaller channels) of 100 and 3000 s^{-1}. When processing at 100 s^{-1}, the first convergence reduced the area of the smallest initial agglomerates from $3.6x10^5$ μm^2 to 1000 μm^2, which is quite significant. Thus, even at this relatively low shear rate, the hydrodynamic stresses generated overcame the cohesive strength of the agglomerates. Subsequently, dispersion proceeded gradually, but once a certain residence time (corresponding to attaining pair 4) was reached, faster dispersion was triggered. After smaller agglomerates were formed, little progress was detected downstream. Probably, higher hydrodynamic stresses and/or longer residence times would be required. Processing at 3000 s^{-1} cut the size of the agglomerates existing after the first convergence down to approximately half the size of those measured at 100 s^{-1}. This was followed by a more gradual dispersion until reaching dispersion levels similar to those obtained at 100 s^{-1}. These observations correlate well with the predictions of the model proposed by Scurati et al [49]: i) the rate of dispersion increases with the intensity of the hydrodynamic stresses generated, as these increase with increasing shear rate; ii) since the probability for break-up is proportional to the residence time and the agglomerate surface area, at constant stress the smaller the agglomerate the longer the exposure time required to break it. Jamali et al. [54] observed that the decrease in electrical resistivity along the length of the mixer followed qualitatively the same behavior as that of the average agglomerate size, albeit with a horizontal shift to higher number of pairs of rings. Thus, a correlation could be established between level of dispersion and electrical resistivity, at constant filler %. In this study a composite consisting of PP and 4 wt.% of CNT formed an electrically conductive network when at least 50% of the surviving agglomerates reached an area smaller than 2000 μm^2.

Figure 9.5b shows dispersion data analogous to that of Figure 9.5a, collected along the axis of a small-size co-rotating twin screw extruder fitted with sample collecting devices [55]. The screws contain a number of conveying elements separated by a small positive helix angle element upstream that induces melting of the PP, and by a kneading zone comprising eight kneading disks staggered at -45º. The conveying sections before these two restrictive regions work partially filled, except for a short length upstream of the kneading zone and of the die, in order to generate the pressure required for axial melt progression. The Figure

shows that most of the dispersion level reached takes place along the first half of the extruder, up to the beginning of the kneading zone, minor changes being measured until the die exit. Upstream and along the kneading block significant hydrodynamic stresses are generated, together with a complex 3D flow favoring intense surface contact renewal. However, further dispersion along the kneading block and during flow in the die would probably require higher stresses, which are difficult to generate as viscous dissipation becomes increasingly important, as well as longer residence times. The three curves in Figure 9.5b demonstrate the role of cohesive strength and interfacial bonding on dispersion [55]. The lowest dispersion was achieved with the as received CNT (curve labelled CNT). The use of chemically functionalized CNT [58] lead to the formation of smaller CNT agglomerates, improving dispersion (label CNT250). Further covalent bonding of PP modified with maleic anhydride (PP-g-MA) to the chemical groups on CNT250 (label CNT250/PP-g-MA) to produce CNT strongly bonded to PP-g-MA molecules, lead to the formation of even smaller agglomerates and thus even higher dispersion level.

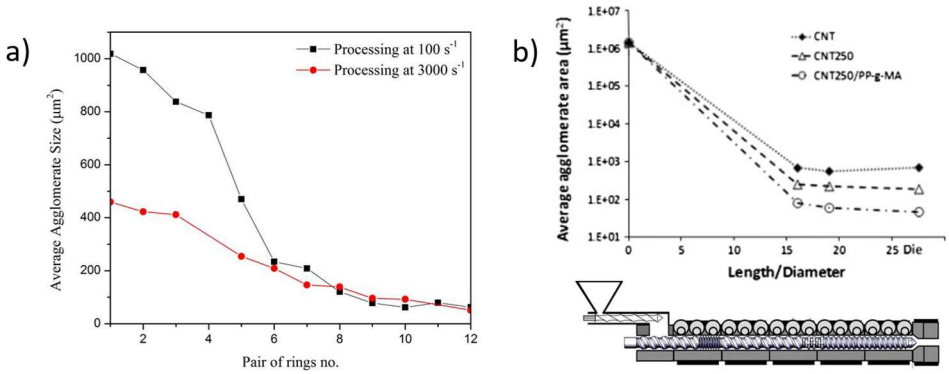

Figure 9.5 Evolution of the CNT agglomerates dispersion in polypropylene along the length of a mixer: a) prototype extensional mixer (adapted from [54]; b) co-rotating twin screw extruder (CNT denotes as received powder, CNT250 and CNT250/PP-g-MA were functionalized as explained in the text (adapted from [55]).

The stability of the dispersion level reached upon thermal annealing, or during an additional thermomechanical cycle, has also been addressed. Coarsening of nanoparticle agglomerates suspended in polymer matrices during thermal annealing has been reported [59-61]. Ma et al. [62] observed that pristine CNT tended to re-agglomerate during curing of epoxy, although the CNT functionalization with amine groups prevented the process. Liu et al. [63] used coarse-grained molecular dynamics to predict that the extent of agglomeration decreases with increasing polymer-filler interaction. The manufacture (i.e., compounding) of a polymer/CNT nanocomposite and its processing (often by extrusion, or injection moulding) into a final product are generally carried out separately and by different players. This implies that after the nanocomposite material is produced, it will be subject to a second thermomechanical cycle, the latter being performed under distinct conditions from those applyed during the first mixing process. For example, evidence of secondary agglomeration during mixing of polycarbonate/CNT was reported by Pegel et al. [39] that resulted in enhancement of the composite electrical conductivity. The viscoelastic recovery of the composite melt involved a fast process, probably related to reagglomeration, and a very slow process caused by the rearrangement of a network structure [64].

Jamali et al [54] studied the effects of processing and reprocessing on agglomerate dispersion using the prototype extensional mixer mentioned above, consisting of a vertical stack of circular channels with alternating small/large diameters. As depicted in the vertical series of micrographs on the left in Figure 9.6, a fine dispersion was progressively obtained after repetitive converging/diverging flows through 12 pairs of rings. The corresponding reduction of average agglomerate area is graphically presented in Fig Fig.9.5a (curve for processing at 3000 s^{-1}). Once extruded and cooled down to room temperature, the material was pelletized, re-heated in the reservoir of the capillary rheometer and reprocessed. As seen in the column of micrographs immediately at the right of the mixer, when reprocessing was carried out under the same average shear rate of 3000 s^{-1}, the evolution of morphology mimics closely that of processing. This means that, as the material was re-heated and kept under quiescent conditions in the reservoir of the rheometer, re-agglomeration took place, reforming agglomerates with sizes similar to those of the initial clusters. When reprocessing was performed at a smaller shear rate than that used for processing (100 s^{-1}) reagglomeration took place as described above, however the agglomerates size remained almost unchanged as the composite melt progressed along the mixer. Under these reprocessing conditions the final extrudate exhibited a coarser morphology than that obtained after the first processing step, as illustrated in the vertical sequence of micrographs at the far right of Figure 9.6. In this case, upon re-heating the material recovered approximately its initial state; when subject to a stress level smaller than that applied during processing (i.e., corresponding to smaller fragmentation number) the dispersion was hindered. In this series of experiments, reprocessing under lower shear rates did not bring about benefits in terms of electrical conductivity, while reprocessing under identical shear rate yielded similar conductivity results.

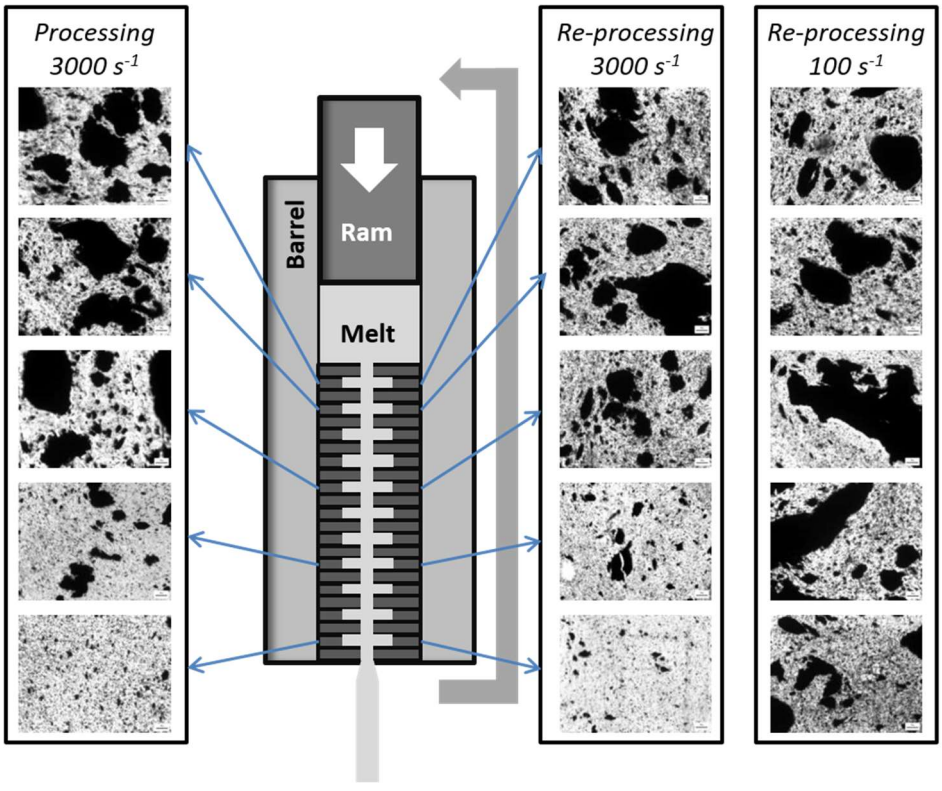

Figure 9.6 Effects of processing and reprocessing at two different shear rates on agglomerate dispersion in polypropylene using a prototype extensional mixer (adapted from [54]).

9.4 Graphene Derivatives

Graphene is a 2-D layer of sp^2 hybridized carbon atoms forming an hexagonal lattice with open edges. It has physical and mechanical properties that are similar or superior to those of CNT, such as Young's modulus of 1 TPa and tensile strength of 125 GPa, electrical conductivity of 10^7 - 10^8 S/m and thermal conductivity around 5 000 $Wm^{-1} K^{-1}$ [65]. Graphene has a higher surface-to-volume ratio compared to CNT since the inner surface of the latter are not accessible to the polymer molecules [66] and an ultra-high aspect ratio (600–10,000). Graphene is a wonder reinforcing material for composite applications, presenting such excellent mechanical, electrical and thermal properties, in addition to high optical transparency. However it is quite difficult to obtain in bulk quantities, as required for composite applications. Graphene and its derivatives may be synthesized through different strategies, including bottom-up methods such as chemical vapor deposition (CVD) growth on selected metal surfaces and synthesys of graphene nanoribbons (GNR) from small aromatic molecules [67], or by top-down methods based on the formation of graphene from graphite, such as formation of graphene oxide (GO) and reduced graphene oxide (rGO), the exfoliation of graphite to form few-layer graphene (FLG) and graphite nanoplates (GNP), graphene quantum dots (GQD), etc [68].

Graphite is the most thermodynamically stable form of carbon under normal conditions. It is constituted by stacks of graphene layers that strongly interact with each other presenting an interlayer spacing of 0.335 nm. Although crystalline graphite is an interesting material itself, being soft (1 in the Mohs hardness scale) but stiff and presenting high electrical (of the order of 10^6 Ω cm^{-1}) and thermal (approximately 400 W $m^{-1} K^{-1}$) conductivities [69], its individual particles are micron-sized, and the material presents a relatively low surface area. A coarser exfoliation of graphite is achieved by intercalation with an alkali metal, alkali earth metal, rare earth metal for donors and metal halides, halogen and acids for acceptors [70-72]. Most of the graphite flakes obtained by these procedures have a thickness from 0.34 to 100 μm [73]. The graphite grades presenting thinner flakes may be denoted as graphite nanoplates (GnP) due to the nanometric flake thickness [74]. These materials can be acquired in large quantities and are thus interesting for composite reinforcement.

Similarly to CNT, GnP tend to form cohesive agglomerates due to the Van der Waals interactions between individual platelets. The agglomerates dispersion in polymers is difficult, and is aggravated by the lack of chemical functionalities at the surface and edges that could provide interfacial bonding with the polymer. Thus, tailored chemical functionalization of the graphene surface may significantly enhance the GnP/polymer interfacial strength [75-77]. Solution blending and in situ polymerization associated to sonication are reportedly more efficient than melt mixing [78-82] and are widely adopted in the scientific literature, but involve the use of solvents and are often difficult to scale-up to industrial production. Also, slow solvent evaporation induces particle reagglomeration and precipitation [83].

9.1.1 Dispersion mechanism

There is abundant literature on the topic of graphene synthesis and graphite exfoliation (e.g. [84,85]), but the kinetics and dispersion mechanism of GnP in polymer melts are not yet well understood. Potts et al [86] observed that both graphite and GO have a layered structure analogous to that of certain silicates (e.g., montmorillonite) and postulated that the two types of materials could be characterized by similar states of dispersion - stacked, intercalated, or exfoliated, as illustrated in Fig. 9.7 - that depend on the mixing technique and affinity between the phases. Phase separation results in a microcomposite, while both intercalated and exfoliated dispersion generate a nanocomposite. Intercalation increases the interfacial

area between the polymer and GNP compared to a phase separated morphology. As seen above, exfoliation would be very hard to achieve, since the required high shear and/or extensional stresses and mixing times would induce thermal degradation effects. In the exfoliated state the orientation of the graphene sheets would determine certain properties such as barrier performance, enhanced by the perfect alignment parallel to the film surfaces, as well as mechanical and electrical properties.

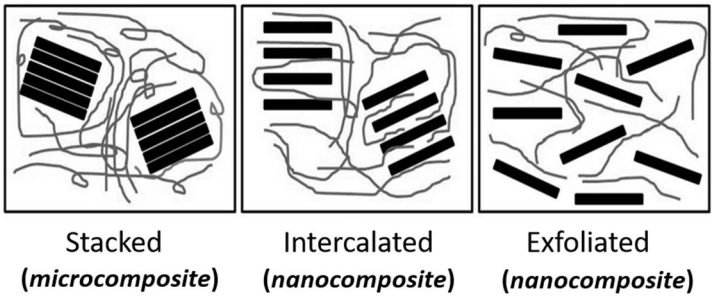

Figure 9.7 Schematic representation of the polymer-GnP morphologies that can result from the dispersion by melt mixing of GnP in polymer matrices (by analogy with polymer-layered organoclay morphologies).

Investigation of correlations between melt compounding methods, their processing parameters and resulting properties of the nanocomposites yielded some insight into the effect of processing conditions upon GnP dispersion. Various of these studies were performed using a vertical co-rotating twin-screw microextruder (DSM Xplore, The Netherlands), which allows to set independently the screw speed, operating temperature and mixing time [87,88]. Higher degree of GnP dispersion was observed under lower melt temperature and higher screw speed. However, within the melt mixing conditions studied, exfoliation to individual or FLG could not be achieved. Muller et al. [88] studied the reinforcing effect of GnP with different particle size and geometry in polycarbonate, reporting that lamellar GnP potenciates lower composite electrical percolation threshold, lower permeability and higher mechanical reinforcement, while compact GnP particles increased the composite thermal conductivity.

Khanam et al. [89] used a laboratorial Brabender co-rotating twin screw extruder to produce LLDPE/GnP nanocomposites. Increasing the extruder screw speed resulted in better dispersion, but could eventually lead to a reduction in viscosity, which was attributed to thermal degradation and/or chain scission. Thus, they concluded that screw speed has a relevant influence in GnP/polymer composite properties and should be optimized. The authors also reported that LLDPE initiates degradation at a low temperature, while LLDPE/GnP degradation starts at higher temperatures. Moreover, they observed that increasing screw speed raised the composite degradation temperature, and associated this effect with the enhanced GnP dispersion that formed a more effective barrier to the degradation products. Shahdan et al [90] prepared Polylactic Acid/Liquid Natural Rubber/GnP nancomposites using a Haake Rheomix internal mixer. They observed that too high or too low speeds would induce agglomeration of the filler in the matrix. Too short mixing times would hinder proper dispersion, whilst long mixing time would lead to oxidation of NR, and chain scission in the PLA. Thus the general trends of dispersion seem to hold regardless of the mixing equipment utilized.

9.1.2 Monitoring the development of dispersion

The authors monitored the development of dispersion of GnP in a PP matrix adopting the approach discussed above for CNT, i.e., using a prototype small-scale extensional mixer attached to a capillary rheometer [91-93]. The geometry of the mixer was modified in order to monitor nanoparticle dispersion and eventual re-agglomeration effects in a single step, without the need to cool the composite, pelletize and re-melt [92,93]. The new mixer version comprised a first mixing zone, a low shear chamber (where the melt is subjected to quasi-quiescent conditions) and a second mixing zone. The first mixing zone mimics the conventional compounding stage, whereas the second mixing zone is equivalent to processing a previously compounded material. The first mixing zone consists of a vertical stack of ten circular rings with alternating internal diameters (1 and 8 mm), thus creating a series of five converging/diverging (8:1 and 1:8) channels. The low shear zone is 24 mm long and has a diameter of 18 mm. The second mixing zone comprises another series of five sequential converging/diverging flows that can be identical or different to the first mixing zone. The assemblage of rings is mounted inside a sleeve that can be quickly unscrewed from the main body of the device and cooled, in order to collect the material inside each channel.

Fig. 9.8a shows the evolution of GnP dispersion along the mixer in terms of the agglomerate area ratio, at three ram speeds [92]. Agglomerate area ratio (Ar) is frequently used as a global dispersion index and represents the fraction of the composite area occupied by agglomerates relative to the overall composite area analyzed. The evolution of dispersion appears to be independent of ram speed, except at the intermediate chamber. This means that the threshold stress for rupture or erosion of the agglomerates was attained even at the lowest ram speed and that the non-Newtonian character of the flow reduces the effect of variations in shear rate. Also, the progress of dispersion along the first mixing section seems to be essentially linear, which contrasts with the behavior of PP/CNT composites prepared in the same type of device (see Fig 9.5), where a stepwise evolution was observed. The latter was taken as evidence of rupture of the CNT agglomerates after a certain mixing time. In the case of GnP, it is difficult to distinguish whether erosion, rupture into progressively smaller agglomerates, or a combination of both prevails. As soon the material flows inside the low shear chamber significant re-agglomeration begins to take place, with Ar regaining values near to those measured in the reservoir. The lower the ram speed (i.e., the higher the residence time), the higher the Ar attained toward the end of this chamber. Thus, during flow under sufficiently low rates, the cohesion forces become predominant over the hydrodynamic stresses and if sufficient residence time is provided, re-agglomeration can be significant. Upon entering the second mixing zone, substantial reduction of Ar is initially observed, but a linear progress is soon regained, although at a slower pace than in the first mixing zone. In a few experiments (with higher filler concentration, not shown in the figure), the final value of Ar at the mixer outlet was higher than that at the exit of the first mixing zone. Fig 9.8b illustrates the effect of surface functionalization of GnP on dispersion. For this purpose, the as-received graphite nanoplates were chemically modified via 1,3-dipolar cycloaddition of azomethine ylides, to form pyrrolidine-functionalized GnP (fGnP) [58]. PP-g-MA was then grafted onto the fGnP surface yielding PP-functionalized GnP (fGnP-PP). These reactions did not significantly change the GnP agglomerate morphology. The figure clearly shows that the progress of dispersion along the mixer for both as received and fGnP-PP is qualitatively similar, but the latter consistently displays lower values of Ar. This improvement in dispersion was attributed to a decrease in the agglomerate cohesion, which was explained by the fact that the PP molecules chemically bonded to the surface of the fGnP-PP increase the equilibrium distance between neighbouring GnP, thus decreasing the van der Waals interactions responsible for their cohesion.

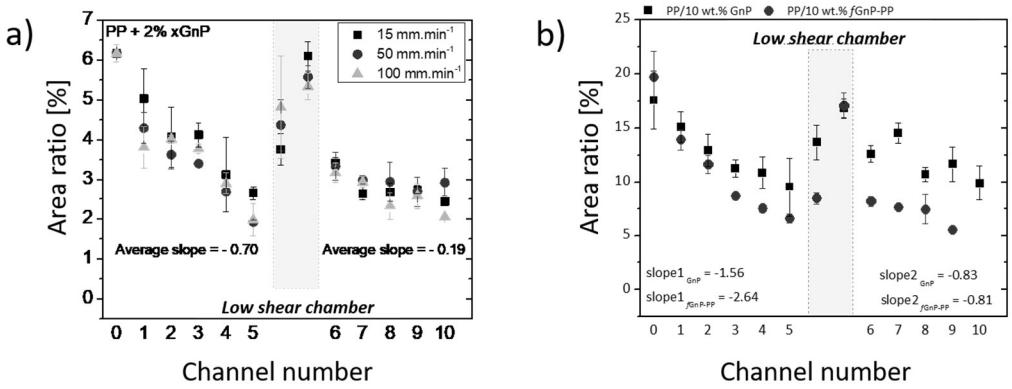

Figure 9.8 Evolution of Area ratio (Ar) along an extensional mixer containing two mixing zones separated by a low shear chamber, for PP/ 2 wt% GnP nanocomposites: (a) effect of ram speed (adapted from [92]); (b) effect of surface functionalization (adapted from [93]).

Figure 9.8 shows that the slope of the Ar variation along the second mixing zone is smaller than that measured along the first mixing zone (similar observations were made for higher filler concentration, REF). This is unexpected, since both mixing zones have exactly the same design, thus generating the same shear rates and residence time. In terms of fragmentation number, this would mean that either lower hydrodynamic stresses were generated in the second mixing section or the cohesive strength of the agglomerates formed along the second shear chamber is higher. Since the former is difficult to account for, Santos et al [93] speculated that the morphology and/or cohesion of the initial GnP agglomerates and of the agglomerates resulting from re-agglomeration may be distinct. The latter could eventually consist of smaller cohesive particles loosely attached to each other, but appearing as large agglomerates under microscopy observation. In the second mixing zone, these particles would quickly detach from each other, but the probability of further rupture would be lower. This sequence is schematized in Fig. 9.9.

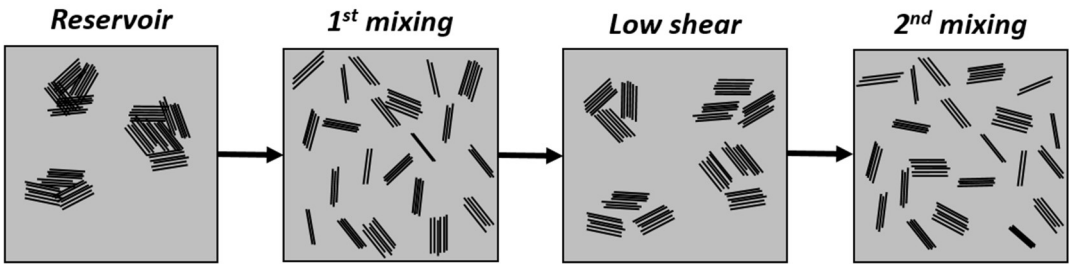

Figure 9.9 Schematic representation of the possible evolution of polymer-GnP morphologies along the prototype extensional mixer.

9.2 CONCLUSIONS

Understanding the dispersion mechanisms of nanoparticles in polymers during melt mixing is a relevant topic, both scientifically and technically. It is essential for the successful production of nanocomposites with tailored properties at minimum expense of nanomaterials. The topic is complex, since the dispersion of nanoparticles in polymer melts is influenced by a variety of factors related to the properties of the components and to processing parameters.

Nanomaterials with diverse chemical composition and different shape will tend to form agglomerates with distinct cohesion and stability, presenting challenges towards the dispersion in polymers. Moreover, the processing and reprocessing conditions may allow significant nanoparticle reagglomeration, thus reverting to a variable extent the dispersion state reached previously.

Here, the dispersion of layered silicates, carbon nanotubes and graphene derivatives in polymer melts were discussed. Studies of the monitoring of dispersion along the melt mixing equipment were presented. The dispersion of organoclays in polymers produced intercalated and exfoliated nanocomposites. It was shown that the clay galleries may collapse, at least partially, due to continuing shear and surfactant degradation, accounting for the reagglomeration effects observed. Reagglomeration effects were also reported for the dispersion of carbon nanotubes and graphite/graphene derivatives, however in this case they were triggered by lower levels of hydrodynamic stresses.

REFERENCES

[1] ISO/TS 80004-2:2015, Nanotechnologies - Vocabulary - Part 2: Nano-objects

[2] Bhattacharya, M., *Materials* (2016) 9, pp. 262-297

[3] Sinha Ray, S., *Clay-Containing Polymer Nanocomposites - From Fundamentals to Real Applications* (2013) Elsevier, Amsterdam

[4] Choi, H.J., Kim, S.G., Hyun, Y.H., Jhon, M.S., *Macromol Rapid Commun* (2001) 22, pp. 320-325

[5] Ogata, N., Kawakage, S., Ogihara, T., *J Appl Polym Sci* (1997) 66, pp. 573-581

[6] Dennis, H. R., Hunter, D. L., Chang, D., Kim, S., White, J. L., Cho, J. W., Paul, D. R., *Polymer* (2001) 42, pp. 9513-9522

[7] Bousmina, M., *Macromolecules* (2006) 39, pp. 4259-4263

[8] Alexandre, M., Dubois, P., *Mater. Sci. Eng.* (2000) 28, 1-63

[9] Utracki, L.A., *Clay-Containing Polymer Nanocomposites* (2004) vol. 1, Rapra Technology Limited

[10] Gupta, R.K., Kennel, E., Kim, K., *Polymer Nanocomposites Handbook* (2010) CRC Press.

[11] Cho, J.W., Paul, D.R., *Polymer* (2001) 42 (3), pp. 1083-1094

[12] Lertwimolnun, W., Vergnes, B., *Polym. Eng. Sci.* (2006) 46 (3) pp. 314-323

[13] Lertwimolnun, W., Vergnes, B., *Polym. Eng. Sci.* (2007) 47 (12) pp. 2100-2109

[14] Lin, B., Thümen, A., Heim, H.-P., Scheel, G., Sundararaj, U., *Polym. Eng. Sci.* (2009) 49, pp. 824-834

[15] Domenech, T., Peuvrel-Disdier, E., Vergnes, B., *Int. Polym. Process.* (2012) 27, pp. 517-526

[16] Fasulo, P.D., Rodgers, W.R., Ottaviani, R.A., Hunter, D. L., *Polym. Eng. Sci.* (2004) 44, pp. 1036-1045

[17] Scatteia, L., Scarfato, P., Acierno, D., *e-Polymers* (2006) 6, 1, 023

[18] Zhu, L., Xanthos, M., *J. Appl. Polym. Sci.* (2004) 93, pp. 1891-1899

[19] Giraldi, A.L.F., Bizarria, M.T.M., Silva, A.A., Velasco, J.I., d'Ávila, M.A., Mei, L.H.I., *J. Appl. Polym. Sci.* (2008) 108, pp. 2252-2259

[20] Shah, R.K., Paul, D. R., *Polymer* (2006) 47, 11, pp. 4075-4084

[21] Treece, M.A., Zhang,W., Moffit, R.D., Oberhauser, J.P., *Polym. Eng. Sci.* (2007) 47, pp. 898-911

[22] Machado, A.V., Covas, J.A., van Duin, M., *J. Appl. Polym. Sci.* (1999) 71, pp. 135-141

[23] Barbas, J.M., Machado, A.V., Covas, J.A., *Chem. Eng. Sci* (2013) 98, pp. 77-87

[24] Mould, S., Barbas, J., Machado, A.V., Nóbrega, J.M., Covas, J.A., *Polym. Testing* (2011) 30, pp. 602-610

[25] Tanoue, S., Utracki, L.A., Garcia-Rejon, A., Ttibouet, J., Cole, K.C., Kamal, M.R., *Polym. Eng. Sci.* (2004) 44, pp. 1046-1060

[26] Xu, L., Nakajima, H., Manias, E., Krishnamoorti, R., *Macromolecules* (2009) 42 (11) pp. 3795-3803

[27] Barbas, J.M., Machado, A.V., Covas, J. A., *J. Applied Polymer Science* (2012) 127, pp. 4899-4909

[28] Yan, L., Roth, C.B., Low, P.F., *Langmuir* (1996) 12, pp. 4421-4429

[29] IJdo, W.L., Kemnetz, S., Benderly, D., *Polym. Eng. Sci.* (2006) 46, pp. 1031-1039

[30] Cole, K.C., *Macromolecules* (2008) 41, pp. 834-843

[31] Nassar, N., Utracki, L.A., Kamal, M.R., *Int. Polym. Process.* (2005) 20, pp. 423-431

[32] Machado, A.V., Barbas, J.M., Covas, J.A., In *Synthesis Techniques for Polymer Nanocomposites: Polymer Nano-, Micro- and Macrocomposites.* Mittal, V. (Ed.) (2015) Wiley-VCH Verlag GmbH & Co. KgaA, Weinheim, Germany, pp. 241-266

[33] Long, Y.Z., Li, M.M., Gu, C., Wan, M., Duvail, J.L., Liu, Z., et al, *Prog. Polym. Sci.* (2011) 36, pp. 1415-1442

[34] De Volder, M.F.L., Tawck, S.H., Baughman, R.H., Hurt, A.J., *Science* (2013) 339, pp. 535-539

[35] Singh, V., Joung, D., Zhai, L., Das, S., Khondaker, S. I., Seal, S., *Progress in Materials Science* (2011) 56 (8), pp. 1178-1271

[36] Liu, J., Tang, J., Gooding, J. J., *J. Mater. Chem.* (2012) 22, pp. 12435- 12452

[37] Alig, I., Pötschke, P., Lellinger, D., Skipa, T., Pegel, S., Kasaliwal, G., Villmow, T., *Polymer* (2012) 53, pp. 4-28

[38] Sathyanarayana, S., Hubner, C., In *Structural Nanocomposites, Engineering Materials.* Njuguna, J., (Ed.) (2013) Springer, Berlin Heidelberg, pp. 19–60

[39] Pegel, S., Potschke, P., Petzold, G., Alig, I., Dudkin, S. M., Lellinger, D., *Polymer* (2008) 49, 974–984

[40] Krause, B., Pötschke, P., Häußler, L., *Composites Science and Technology* (2009) 69, pp. 1505-1515

[41] Krause, B., Mende, M., Pötschke, P., Petzold, G., *Carbon* (2010) 48, pp. 2746-2754

[42] Socher, R., Krause, B., Müller, M. T., Boldt, R., Pötschke, P., *Polymer* (2012) 53, pp. 495–504

[43] Salzano de Luna, M., Pellegrino, L., Daghetta, M., Mazzocchia, C.V., Acierno, D., Filippone, G., *Composites Science and Technology* (2013) 85, pp. 17–22

[44] Huang Y.Y., Terentjev, E.M., *Polymers* (2012) 4 (1), pp. 275-295

[45] Bhattacharyya, A.R., Sreekumar, T.V., Liu, T., Kumar, S., Ericson, L.M., Hauge, R.H., *Polymer* (2003) 44, pp. 2373–2377

[46] Hwang, T.Y., Kim, H.J., Ahn, Y., Lee, J.W., *Korea-Aus. Rheol. J.* (2010) 22, pp. 141–148

[47] Pan, Y., Chan, S.H., Zhao, J., *Composites Part A* (2010) 41, pp. 419–426

[48] Kasaliwal, G.R., Villmow, T., Pegel, S., Pötschke, P., In *Polymer–Carbon Nanotube Composites – Preparation, Properties and Applications.* McNally, T., Pötschke, P. (Eds.) (2011) Series in Composites Science and Engineering, Woodhead Publishing, Cambridge, UK, pp. 92– 132

[49] Scurati, A., Feke, D.L., Manas-Zloczower, I., *Chem. Eng. Sci.* (2005) 60, pp. 6564 – 6573

[50] Domingues, N., Gaspar-Cunha, A., Covas, J.A., Camesasca, M., Kaufman, M., Manas-Zloczower, I., *Int. Polym. Proc.* (2010) 25, pp. 188–198

[51] Villmow, T., Pötschke, P., Pegel, S., Haussler, L., Kretzschmar, B., *Polymer* (2008) 49, pp. 3500-3509

[52] Kasaliwal, G.R., Pegel, S., Göldel, A., Pötschke, P., Heinrich, G., *Polymer* (2010) 51, pp. 2708–2720

[53] Novais, R.M., Covas, J.A., Paiva, M.C., *Composites: Part A* (2012) 43, pp. 833–841

[54] Jamali, S., Paiva, M.C., Covas, J.A., *Polym. Testing* (2013) 32, pp. 701–707

[55] Novais, R.M., Simon, F., Paiva, M.C., Covas, J.A, *Composites Part A* (2012) 43, pp. 2189–2198

[56] Nguyen, X.Q., Utracki, L. A., US Patent 5451106 (1995)

[57] Utracki, L.A., Luciani, A., Bourry, D.J.J., US Patent 6550956, B1 (2003)

[58] Paiva, M.C., Simon, F., Novais, R., Ferreira, T., *ASC Nano* (2010) 4 (12) pp. 7379-7386

[59] Filippone, G., Romeo, G., Acierno, D., *Langmuir* (2010) 26, pp. 2714–2720

[60] Jia, X. L., Listak, J., Witherspoon, V., Kalu, E.E., Yang, X.P., Bockstaller, M.R., *Langmuir* (2010) 26, pp. 12190–12197

[61] Kiel, J.W., Eberle, A.P.R., Mackay, M.E., *Phys. Rev. Lett.* (2010) 105, pp. 168701-168701-4

[62] Ma, P.C., Mo, S.-Y., Tang, B.-Z., Kim, J.-K., *Carbon* (2010) 48, pp. 1824–1834

[63] Liu, J., Gao, Y., Cao, D., Zhang, L., Guo, Z., *Langmuir* (2011) 27, pp. 7926–7933

[64] Richter, S., Saphiannikova, M., Jehnichen, D., Bierdel, M., Heinrich, G., *eXPRESS Polym. Lett.* (2009) 3, pp. 753–768

[65] Sur, U. K., Graphene: A Rising Star on the Horizon of Materials Science, *Int. J. Electrochem.* (2012) ArticleID 237689, 12 pages

[66] Hu, K., Kulkarni, D.D., Choi, I., Tsukruk, V.V., *Progress in Polymer Science* (2014) 39, pp. 1934-1972

[67] Talirz,L., Söde, H., Cai, J., Ruffieux, P., Blankenburg, S., Jafaar, R., Berger, R., Feng, X., Müllen, K., Passerone, D., Fasel,R., C.A., J. *Am. Chem. Soc*. (2013) 135, pp. 2060−2063

[68] Wick, P., Louw-Gaume, A.E., Kucki, M., Krug, H.F., Kostarelos, K., et al., *Angewandte Chemie International Edition*, (2014) 53, 30, pp. 7714-7718

[69] Randviir, E.P., Brownson, D.A.C., Banks, C.E., *Mater. Today* (2014) 17, pp. 426–432

[70] Potts, J. R., Dreyer, D. R., Bielawski C. W., Ruoff, R. S., *Polymer* (2011) 52, pp. 5–25

[71] Selig H., Ebert, L.B., In *Advances in Inorganic Chemistry and Radiochemistry*, Emeleus H. J., Sharpe, A.G. (Eds.) (1980) Academic Press, 23, pp. 281–327

[72] Vogel, F.L., US Patent 4565649 (1986)

[73] Bunnell, L.R., US Patent 5186919 (1993)

[74] Bianco, A., Cheng, H.-M., Enoki, T., Gogotsi, Y., Hurt, R. H., Koratkar, N., Kyotani, T., Monthioux, M., Park, C.R., Tascon J.M.D., Zhang, J., *Carbon* (2013) 65, pp. 1–6

[75] Bai, H., Li, C., Shi, G., *Adv. Mater*. (2011) 23, 1089-1115

[76] Ma, J., Meng, Q., Zaman, I., Zhu, S., Michelmore, A., Kawashima, N., Wang, C., Kuan, H., *Compos. Sci. Technol*. (2014) 91, pp. 82-90

[77] Naebe, M., Wang, J., Amini, A., Khayyam, H., Hameed, N., Li, L., Chen, Y. Fox, B., *Scientific Rep.* (2014) 4, 4375, 7 pages

[78] Huang, X., Qi, X., Boey, F., Zhang, H., *Chem. Soc. Rev.* (2012) 42, pp. 666-686

[79] Das T., Prusty, S., *Polym. Plast. Technol. Eng.* (2013) 52, pp. 319-331

[80] Saravanan, N., Rajasekar, R., Mahalakshmi, S., Sathishkumar, T.P., Sasikumar, K.S.K., Sahoo, S., *Journal of Reinforced Plastics and Composites* (2014) 33, pp. 1158-1170

[81] Kim, H., Miura, Y., Macosko, C.W., *Chem. Mater.* (2010) 22, pp. 3441-3450

[82] Galindo, B., Alcolea, S.G., Gómez, J., Navas, A., Murguialday, A.O., Fernandez, M.P., Puelles, R.C., *IOP Conf. Series: Materials Science and Engineering* (2014) 64, 012008, 6 pages

[83] Cui, Y., Kundalwal, S.I., Kumar, S., *Carbon* (2016) 98, pp. 313-333

[84] Cai, M., Thorpe, D., Adamsonb D.H., Schniepp, H.C., *J. Mater. Chem.* (2012) 22, pp. 24992-25002

[85] Lin, Z., Karthik, P.S., Hada, M. Nishikawa, T., Hayashi, Y., Nanomaterials (2017) 7, pp. 125, 10 pages

[86] Potts, J.R., Dreyer, D.R., Bielawski, C.W., Rodney, S.R., *Polymer* (2011) 52, pp. 5-25

[87] Sullivan, E.M., Gerhardt, R.A., Wang, B., Kalaitzidou, K., *J. Mater. Sci.* (2016) 51, pp. 2980-2990

[88] Müller, M.T., Hilarius, K., Liebscher, M., Lellinger, D., Alig, I., Pötschke, P., *Materials* (2017) 10, pp. 545, 23 pages

[89] Khanama, P.N., AlMaadeed, M.A., Ouederni M., Harkin-Jones, E., Mayorae, B., Hamilton, A., Sun, D., *Vacuum* (2016) 130, pp. 63-71

[90] Shahdan, D., Ahmad, S.H., Chen, R.S., Ali, A.M., Zailan, F.D., *AIP Conference Proceedings* (2016) 1784, 040017

[91] Vilaverde, C., Santos, R.M., Paiva, M.C., Covas, J.A., *Composites Part A* (2015) 78, 143–151

[92] Cunha, E., Paiva, M.C., Hilliou, L., Covas, J.A., *Polym. Composites* (2015) 8 pages, doi: 10.1002/pc.23657

[93] Santos, R.M., Vilaverde, C., Cunha, E.P., Paiva M.C., Covas, J.A., *Soft Matter* (2016) 12, 77-86